arXiv:0809.0644v2 [cond-mat.mtrl-sci] 4 Sep 2008

Interaction of a CO molecule with a Pt monatomic wire: electronic structure and ballistic conductance

Gabriele Sclauzero,[1,2] Andrea Dal Corso,[1,2] Alexander Smogunov,[2,3,4] and Erio Tosatti[1,2,3]

[1] *International School for Advanced Studies (SISSA-ISAS), Via Beirut 2-4, IT-34014 Trieste, Italy*
[2] *CNR-INFM Democritos, Via Beirut 2-4, IT-34014 Trieste, Italy*
[3] *International Centre for Theoretical Physics (ICTP), Strada Costiera 11, IT-34014 Trieste, Italy*
[4] *Voronezh State University, University Sq. 1, 394006 Voronezh, Russia*

(Dated: September 4, 2008)

We carry out a first-principles density functional study of the interaction between a monatomic Pt wire and a CO molecule, comparing the energy of different adsorption configurations (bridge, on top, substitutional, and tilted bridge) and discussing the effects of spin-orbit (*SO*) coupling on the electronic structure and on the ballistic conductance of two of these systems (bridge and substitutional). We find that, when the wire is unstrained, the bridge configuration is energetically favored, while the substitutional geometry becomes possible only after the breaking of the Pt-Pt bond next to CO. The interaction can be described by a donation/back-donation process similar to that occurring when CO adsorbs on transition-metal surfaces, a picture which remains valid also in presence of *SO* coupling. The ballistic conductance of the (tipless) nanowire is not much reduced by the adsorption of the molecule on the bridge and on-top sites, but shows a significant drop in the substitutional case. The differences in the electronic structure due to the *SO* coupling influence the transmission only at energies far away from the Fermi level so that fully- and scalar-relativistic conductances do not differ significantly.

PACS numbers: 73.63.Rt, 73.23.Ad, 73.20.Hb
Keywords: platinum nanowire, carbon monoxide, ballistic conductance, spin-orbit coupling

I. INTRODUCTION

Metallic nanocontacts and nanowires are routinely fabricated by scanning tunneling microscopy (*STM*) or mechanically controllable break-junctions (*MCBJ*).[1] The size of these contacts can be as small as a single atom, so that electron transport through them is ballistic and quantized. The current is carried by quantum channels where electrons are partly transmitted and partly reflected. If perfectly transmitting, each (spin degenerate) channel contributes to the conductance with one quantum unit $G_0 = 2\,e^2/h$. A massive contact of section area A encompasses a channel number $N \propto A$ and a conductance proportional to NG_0.[1,2]

Experimentally one observes that when the contact ends are pulled apart the conductance decreases stepwise, showing plateaus followed by sudden jumps. In general, the values of the conductance plateaus depend on the detailed and uncontrolled contact geometry and electronic configuration, but averaging over many configurations makes it possible to plot conductance histograms which display peaks at most frequent plateau values characteristic of the nanocontact of that particular metal.[1] The lowest conductance peak is generally of order $G_0 = 2\,e^2/h$, thus attributable to a monatomic contact in the likeliest geometry preceding breaking.

Some metals such as gold, platinum and iridium display a tendency to form ultimately thin nanocontacts consisting of short tip-suspended monatomic chains, which have also been visualized by transmission electron microscopy[3,4,5] and/or identified by the presence of very long plateaus in the conductance traces versus pulling distance.[6,7] In these metals the lowest conductance histograms peak(s) thus may generally correspond either to a chain or to a single atom contact. In Au the peak is found at about 1 G_0,[1,3,6] corresponding to a single (spin degenerate) $6s$ channel. In Pt, where in addition to $6s$ electrons, $5d$ electrons contribute to the conductance, the peak is usually found between 1.5 G_0 and 2.0 G_0.[5,7,8,9,10,11]

It has long been recognized that the adsorption of small gas molecules on the nanowire or very near the nanocontact may change substantially the conductance of the system, and thus the position of the peaks in the conductance histograms. For instance, in Pt nanocontacts the presence of H_2 causes the suppression of the peak at 1.5 G_0 and the formation of new peaks at 1 G_0 and 0.1 G_0.[10,12,13] In presence of CO instead, the lowest conductance peak is replaced by two new peaks, a major one just above 1 G_0 and a smaller one at 0.5 G_0.[8,9]

Such adsorption-induced modifications are usually rationalized by guessing a few possible adsorption geometries and calculating, via density functional theory, their Landuaer-Büttiker ballistic conductance.[14] In some cases the structural assignment is further supported by comparison of the calculated and the measured frequencies of the molecular vibrational modes. For instance, in the case of H_2 the peak at 1 G_0 could be attributed to a molecular configuration bridging linearly the two Pt tips,[12] while in the case of CO it was shown theoretically[15] that a conductance value of 0.5 G_0 may be caused by a "tilted bridge" configuration of the CO molecule between two Pt contact atoms. In this case however, the peak at 1 G_0 is still unexplained; besides,

several other questions remain open, calling for further theoretical investigations. To begin with, it remains to be clarified what is the electronic mechanism that binds a CO molecule to a monatomic wire. Experimentally, it has been suggested that the Blyholder model,[16] often used to explain the adsorption of CO on transition metal surfaces[17,18] in analogy with metal-carbonyl systems,[19] could explain the relative strength of CO absorption on Cu, Ni, Pt and Au nanocontacts,[9] but *ab-initio* calculations proving this point are still lacking. Moreover, in the case of heavy atomic species such as Pt and Au it is known that spin-orbit (*SO*) effects will change the electronic structure of nanowires[20,21] (for instance altering the nature and number of conducting channels, or leading a Pt nanowire to become magnetic at distances much shorter than those predicted without the explicit inclusion of *SO* coupling[20]), but it is still unclear how these effects would reflect on the chemical binding of a molecule such as CO to the nanocontact, or on the ballistic conductance of the system.

In order to address some of these points, we will study, via *ab-initio* density functional theory (*DFT*), a simplified model: a monatomic chain of Pt atoms with one CO molecule adsorbed on it. We consider a few possible adsorption geometries and discuss their electronic structure and ballistic conductance (in the absence of tips). The role of *SO* coupling is investigated by comparing the results obtained by scalar-relativistic (*SR*) and fully-relativistic (*FR*) pseudo potentials (*PP*),[22] the latter including the *SO* coupling. Magnetic effects, which also could play a role in this system,[23] are not addressed here and will be the subject of future work, along with the additional effects caused by the tips.

We find that when the wire is unstrained and the nanowire atoms are kept fixed at their theoretical equilibrium distance, adsorption of CO in the bridge site (see Fig. 1 in Sec. II) is energetically favored with respect to absorption on the on-top site. The energy of a configuration where CO is joining two Pt atoms (substitutional configuration) is much higher since the energy cost of breaking the Pt-Pt bond is large. Hence, this configuration could possibly appear only when the Pt-Pt bond close to CO is highly strained and almost broken. At intermediate strains a "tilted bridge" configuration as proposed in Refs. 15,24 could moreover be energetically favorable. In this work we will focus on the upright bridge and substitutional configurations only, two examples with completely different symmetry properties. Only occasional data on the structure and energetics of the on-top and "tilted bridge" geometries will be reported for comparison. More results on the on-top configuration are given in Refs. 25,26.

Our results confirm that the Blyholder model[16] explains quite well the electronic structure in the bridge and on-top geometries. In this model both the HOMO (5σ) and LUMO ($2\pi^\star$) of the molecule form bonding-antibonding pairs with the Pt states, giving rise to the so-called "donation/back-donation" process (part of the 5σ density of states, *DOS*, moves above the Fermi energy, E_F, while part of the $2\pi^\star$ *DOS* moves below E_F). In presence of *SO* coupling this picture retains its validity. The states involved in the donation/back-donation process are still identifiable and are in fact found to be energetically nearly at the same position as in the *SR* case. Similar conclusions are reached in the substitutional case although some features are different from the bridge and top cases.

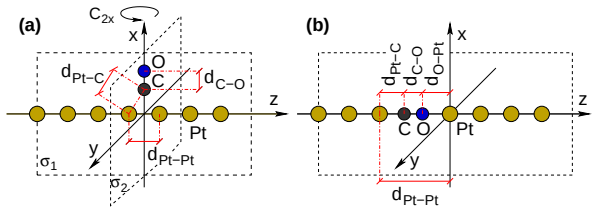

FIG. 1: Schematic representation of the bridge (a) and substitutional (b) geometries with the indication of the distances that are allowed to vary during the geometrical optimization.

The ballistic conductance of our (tipless) system, where the CO adsorbate acts as the scatterer, is found to depend on geometry but is not substantially modified by the introduction of *SO* coupling. The theoretical *SR* (*FR*) conductance is 3.3 G_0 (3.2 G_0) in the bridge configuration, only slightly reduced in comparison to the perfect Pt nanowire (whose theoretical value is 4 G_0, see Ref. 21). In the substitutional geometry we find instead a conductance of 1.1 G_0 (0.9 G_0), thus much smaller than the value of the pristine nanowire. Although tipless results are clearly not directly comparable with experiments, they are consistent with the calculations of Strange et al.[15], which show a large reduction of conductance when the CO passes from the upright bridge to the tilted bridge configuration.

This paper is organized as follows: in Sec. II we briefly describe the methods and some technical details. In Sec. III we discuss the geometry and energetics of the system while in Sec. IV we describe the electronic structure of the bridge and substitutional configurations (Sec. IV A and Sec. IV B, respectively), reporting both the *SR* and *FR* results. The ballistic conductance and the energy-dependent transmission are presented in Sec. V. Finally, in Sec. VI we will draw some conclusions.

II. METHOD

We performed our calculations in the standard framework of density functional theory[27] (*DFT*) using the QUANTUM-ESPRESSO package.[28] We used the local density approximation[29] (*LDA*), with the Perdew and Zunger[30] parametrization of exchange and correlation energy. In addition, optimized geometries and adsorption energies have been also calculated within the generalized gradient approximation (*GGA*), using the functional proposed by Perdew, Burke, and Ernzerhof[31] (*PBE*).

Nuclei and core electrons have been described by Vanderbilt ultrasoft pseudopotentials[32] (*US-PP*), in their scalar-relativistic (*SR*) and fully-relativistic (*FR*) forms. The latter, which include *SO* coupling effects, are used within a two component spinor wavefunctions scheme as described in Ref. 22. *LDA* PP's of Pt are reported in Ref. 33, while both for C and for O we generated *US-PP*.[45] Within *GGA* we generated *SR US-PP* for all the atoms needed for this work.[46] The Kohn-Sham (*KS*) orbitals are expanded in a plane wave basis set with a kinetic energy cut-off of 29 Ry (32 Ry) in the *SR*- (*FR*-) *LDA* case, while a cut-off of 300 Ry has been used for the charge density. In *GGA* calculations (which have been performed only in the *SR* case) we used cut-offs of 32 Ry and 320 Ry. The orbital occupations are broadened using the smearing technique of Methfessel and Paxton[34] with a smearing parameter $\sigma = 0.01$ Ry.

The infinite nanowire has been simulated in a tetragonal cell, with the wire axis along the z direction. The size of the cell along x and y is $d_\perp = 18$ a.u. $\simeq 9.5$ Å, so that the interaction energy between the periodic replicas of the wire is far below 1 mRy. The chemisorption energies $E_{\rm chem}$ (see Sec. III) have been calculated with the same $d_\perp$ and the estimated numerical error is less than a tenth of eV. The nanowire with one adsorbed CO molecule has been simulated by $N_{\rm Pt}$ platinum atoms inside a tetragonal supercell, as shown in Fig. 1 for the bridge and substitutional geometries. A similar supercell has been used also for the on-top and tilted bridge geometries. We checked that the chemisorption energies and optimized distances (reported in Sec. III) are at convergence with $N_{\rm Pt} = 15$, while for the *PDOS* (presented in Sec. IV) we used many more Pt atoms in the supercell. In order to reduce the effects of the periodic CO replicas on the bands, we used $N_{\rm Pt} = 50$ for the *FR PDOS*, and up to $N_{\rm Pt} = 105$ in the *SR* case. The Brillouin zone (BZ) has been sampled with a uniform mesh of k-points along the z direction and the Γ point in the perpendicular directions. In the total energy calculations we used 91 k-points for the clean wire (more than enough to ensure a converge within 1 mRy for the total energy), while we reduced the number of k-points of the supercell according to $N_{\rm Pt}$. The *PDOS* have been calculated employing a uniform mesh of $(1050/N_{\rm Pt})$ k-points, since the size of the BZ reduces linearly with $N_{\rm Pt}$.

The ballistic conductance has been calculated within LDA, in the Landauer-Büttiker formalism, evaluating the total transmission at the Fermi energy. The transmission as a function of energy has been obtained using the method proposed by Choi and Ihm,[35] recently extended to the *US-PP* scheme, both in the *SR* case[36] and in the *FR* case[21] and implemented in the `PWCOND` code (included in the QUANTUM-ESPRESSO package). Since the complex band structure calculation (needed to compute the transmission) is much less sensitive to the periodic replica effects (see Sec. V for more details), we used 17 Pt atoms in the supercell to calculate the ballistic conductance.[47]

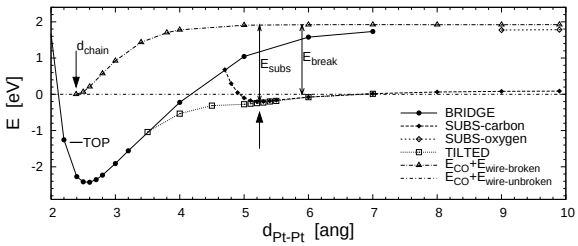

FIG. 2: Optimized energy (with respect to the C and O positions) for different geometries as a function of the Pt-Pt distance, $d_{\rm Pt-Pt}$ (see text). In the BRIDGE (SUBS) geometry, indicated with solid (dashed) line, the C and O atoms are constrained to be on the x (z) axis, while in the TILTED geometry (dotted line) they can move on the whole xz plane. In the SUBS-carbon (-oxygen) the molecule is attached to the Pt atom with the C (O) atom. The optimized energy of the TOP geometry (only at $d_{\rm Pt-Pt} = d_{\rm chain}$) is indicated with an horizontal thick line. The zero of the energy is set as the sum of the energies of an isolated CO and an isolated Pt chain (with the same $N_{\rm Pt}$ and $d_{\rm Pt-Pt} = d_{\rm chain}$). This energy has been calculated also for some values of $d_{\rm Pt-Pt} \geqslant d_{\rm chain}$ (triangles), and at a large enough $d_{\rm Pt-Pt}$ it equals $E_{\rm break}$. The energy gain of placing substitutionally the CO at an already broken Pt-Pt bond is then given by $E_{\rm subs}$ and is comparable to the $E_{\rm chem}$ of CO at the bridge site of an unbroken wire.

III. GEOMETRY AND ENERGETICS

We partially optimized the geometry of the system (see Fig. 1) by moving only the C and O atoms,[48] while keeping the Pt atoms fixed on the z axis. In the bridge and substitutional configurations, this optimization has been repeated for different values of the distance ($d_{\rm Pt-Pt}$) between the two Pt atoms next to CO while all the other Pt atoms are at the theoretical equilibrium distance in the isolated chain ($d_{\rm chain} = 2.34$ Å with *LDA*, $d_{\rm chain} = 2.39$ Å with *GGA*). In the on-top case, only the configuration with all Pt atoms at the theoretical equilibrium distance has been considered. The *GGA* total energy of the optimized configurations is shown as a function of $d_{\rm Pt-Pt}$ in Fig. 2. The zero of the energy has been chosen as the sum of the energies of the isolated CO and of the isolated Pt chain at equilibrium distance (i.e. without broken bonds). In the same plot we report also the sum of the energies of the isolated CO and of a Pt chain with one bond stretched to $d_{\rm Pt-Pt}$.

In Tab. I we report the chemisorption energies, $E_{\rm chem}$, and geometrical parameters calculated for three selected configurations: the on-top geometry with all Pt atoms equally spaced by $d_{\rm chain}$, the bridge geometry at $d_{\rm Pt-Pt} = d_{\rm chain}$, and the substitutional geometry at the optimal $d_{\rm Pt-Pt}$. For the bridge and substitutional *GGA* cases, the values of $E_{\rm chem}$ reported in the table correspond to the energy of the BRIDGE and SUBS-carbon curves in Fig. 2, at the values of $d_{\rm Pt-Pt}$ pointed by the arrows.

If the bond is not stretched ($d_{\rm Pt-Pt} \simeq d_{\rm chain}$), the bridge configuration is favored with respect to the on-

TABLE I: Relaxed distances (in Å) and chemisorption energies (in eV) for the on-top and bridge geometries at $d_{\mathrm{Pt-Pt}} = d_{\mathrm{chain}}$, and for the substitutional geometry at the optimum $d_{\mathrm{Pt-Pt}}$. In the substitutional case, the energy cost for breaking the wire (calculated as described in Fig. 2) is also shown.

	ON-TOP			BRIDGE			SUBSTITUTIONAL				
	$d_{\mathrm{Pt-C}}$	$d_{\mathrm{C-O}}$	E_{chem}	$d_{\mathrm{Pt-C}}$	$d_{\mathrm{C-O}}$	E_{chem}	$d_{\mathrm{Pt-C}}$	$d_{\mathrm{C-O}}$	$d_{\mathrm{O-Pt}}$	E_{chem}	E_{break}
SR-LDA	1.82	1.14	−1.9	1.95	1.16	−2.9	1.82	1.17	2.05	−0.5	2.5
FR-LDA	1.81	1.14	−2.0	1.95	1.16	−3.0	1.82	1.17	2.06	−0.6	2.4
SR-GGA	1.84	1.15	−1.4	1.98	1.17	−2.3	1.85	1.17	2.22	−0.2	1.9

top position, the adsorption energy being about 1 eV smaller for the on-top configuration within both *LDA* and *GGA*. The energy of the bridge as a function of $d_{\mathrm{Pt-Pt}}$ has a minimum at a distance slightly longer than d_{chain} ($d_{\mathrm{Pt-Pt}} = 2.56$ Å in the *GGA* and $d_{\mathrm{Pt-Pt}} = 2.50$ Å in the *LDA*, not shown here). The substitutional geometry has an energy minimum at a much longer distance ($d_{\mathrm{Pt-Pt}} = 5.24$ Å with *GGA* and $d_{\mathrm{Pt-Pt}} = 5.05$ Å with *LDA*). In this hyper-stretched configuration the substitutional geometry is favored with respect to the bridge configuration. However, here a "tilted bridge" configuration, where the CO axis lies on the xz plane but is in not aligned with the x axis or with the z axis, still has an energy slightly lower than the substitutional minimum. While this tilted configuration does not reveal an energy minimum with respect to $d_{\mathrm{Pt-Pt}}$, it is anyway preferred to the bridge and substitutional configurations at intermediate distances (about 3.7 Å $\leqslant d_{\mathrm{Pt-Pt}} \leqslant$ 5.3 Å with *GGA* and 3.8 Å $\leqslant d_{\mathrm{Pt-Pt}} \leqslant$ 5.1 Å with *LDA*).

Although assessing correct binding energies of CO on close-packed Pt surfaces, as the Pt(111) surface and vicinals to it, can be difficult in *DFT* with many of the commonly used exchange and correlation functionals, potentially resulting in a wrong predicted site preference,[37] in the nanowire case the calculated energy difference between bridge and top sites (about 1 eV) is sensibly larger than the potential energy corrugation of that problematic surface case ($\sim 0.1 - 0.2$ eV). Moreover, experimentally CO has been shown to bind to the bridge site of Pt nanowires formed by Pt dimers deposited on a Ge(001) surface,[38] thus partially supporting our prediction for the unsupported nanowire.

In Tab. I we also report the energy cost for breaking a Pt-Pt bond; it is of the order of 1.9 eV within *GGA* (as can be additionally inferred from Fig. 2) and about 2.4 eV within *LDA*. Note that the chemisorption energy of substitutional CO on a broken wire (indicated by E_{subs} in the same figure) is comparable to the chemisorption energy in the bridge configuration. Moreover, as can be seen from Fig. 2 by comparing the two curves SUBS-carbon and SUBS-oxygen at a fixed $d_{\mathrm{Pt-Pt}}$, adsorption on the C side is much more favorable than adsorption on the O side, a standard and chemically obvious finding.[49] (filled diamonds and empty diamonds, respectively).

In all geometries the optimized C-O bond distance is slightly longer than the value $d_{\mathrm{CO,eq}}$ calculated for the isolated molecule, ($d_{\mathrm{CO,eq}} = 1.13$ Å and $d_{\mathrm{CO,eq}} = 1.14$ Å within the *LDA* and *GGA*, respectively). The calculated optimal distance between the C atom and the nearest neighbour Pt atoms, $d_{\mathrm{Pt-C}}$, is about 1.95 Å (1.98 Å) in the bridge geometry within *LDA* (*GGA*); it is longer than the C-Pt distance found in the on-top geometry, $d_{\mathrm{Pt-C}} = 1.82$ Å (1.85 Å). This increase of $d_{\mathrm{Pt-C}}$ with the coordination number of C is in agreement with experimental and theoretical values found for CO adsorbed on Pt(111) surfaces. For instance, LEED experiments report $d_{\mathrm{Pt-C}} \simeq 1.85$ Å for atop CO and $d_{\mathrm{Pt-C}} \simeq 2.08$ Å for CO at the bridge site and *DFT* calculations at the *GGA* level are quite close to these values (see Ref. 39 and references therein). In the substitutional case $d_{\mathrm{Pt-C}}$ is quite similar to the on-top case, while the C-O bond is slightly longer than in the other two geometries. Finally we note that in LDA bonding distances and chemisorption energies do not change significantly in presence of *SO* coupling. This result is in line with the general observation, supported by results in the next Section, that while Fermi-level related properties including transport may be heavily and directly influenced by *SO* coupling through band splittings, the overall energetics, involving charge distributions obtained by integration over the complex of these bands rather than just those at E_F, is much less altered by *SO*.

IV. ELECTRONIC STRUCTURE

In this section we present the electronic structure of the bridge and substitutional geometries (calculated within *LDA*), for the specific configurations pointed by the arrows in Fig. 2 ($d_{\mathrm{Pt-Pt}} = d_{\mathrm{chain}} = 2.34$ Å and $d_{\mathrm{Pt-Pt}} =$ 5.05 Å, respectively). The substitutional geometry preserves the rotational symmetry of the infinite nanowire, and that allows a classification of *SR* (*FR*) states according to the quantum number m (m_j) — the projection of the orbital (total) angular momentum along the wire axis. In the bridge geometry, where the symmetry point group reduces to C_{2v}, this is no longer the case. The C_{2v} symmetry group contains the elements illustrated in Fig. 1 (the identity E, the rotation of π radians about the x axis C_{2x} and the mirror symmetries σ_1 and σ_2), but no rotation along z. We analyze the density of states (*PDOS*) projected onto the atomic orbitals of C, of O and

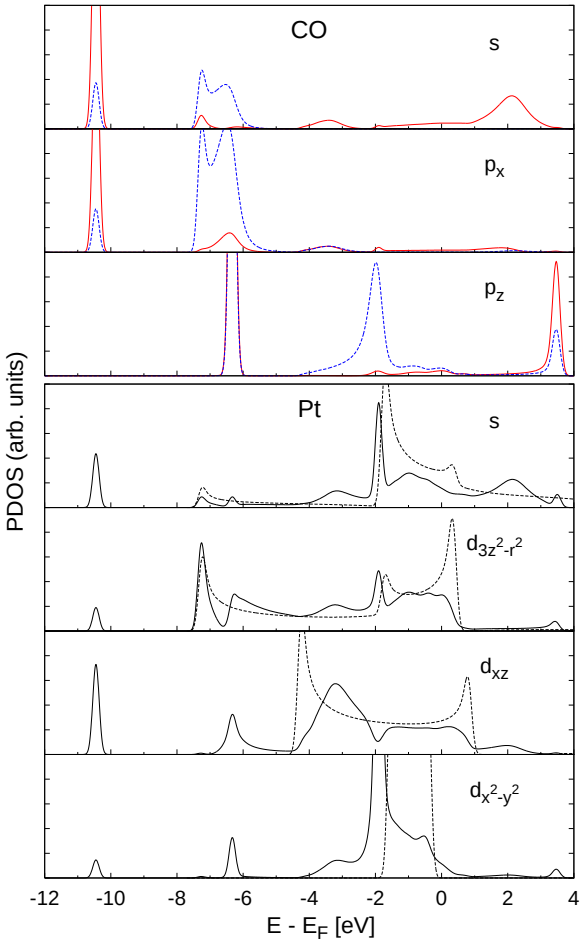

FIG. 3: (Color online) *PDOS* for the *SR-LDA* bridge configuration. In the upper panel we project onto the even atomic orbitals centered on C (solid red lines) and O (dashed blue lines) atoms. In the lower panel the projections are onto the even atomic orbitals of the Pt atoms below the molecule (solid lines). The *PDOS* for the isolated wire are also shown (dashed lines).

of the Pt atoms in contact with CO, separated according to their symmetry. A similar analysis for the on-top geometry is reported in Refs. 25,26.

A. CO adsorbed on the bridge site

We start by discussing the *SR* electronic structure of the Pt nanowire with CO adsorbed at the bridge site when all Pt atoms are equally spaced. For arbitrary k_z the small group of k_z is $C_s = \{E, \sigma_1\}$, thus we can divide the states into "even" and "odd" with respect to the xz mirror plane (σ_1 symmetry in Fig. 1).

We report in Fig. 3 the electronic *PDOS* projected on the *even* atomic orbitals of C and O and on the even atomic orbitals of a Pt atom in contact with CO. The *PDOS* are decomposed into the projections on the s, p_x or p_z orbitals of C and O and into those on the s, $d_{3z^2-r^2}$, d_{xz} or $d_{x^2-y^2}$ orbitals of Pt. Some of the peaks correspond to the even levels of the molecule. The 3σ and 4σ molecular states are in the C and O s and p_x *PDOS*, at -22.5 eV (not shown) and at -10.4 eV, respectively, while peaks corresponding to the 1π and to the $2\pi^*$ states are at about -6.3 eV and at 3.3 eV in the C and O p_z *PDOS*. The 4σ state is slightly hybridized with the even Pt orbitals, while the 3σ state is not.

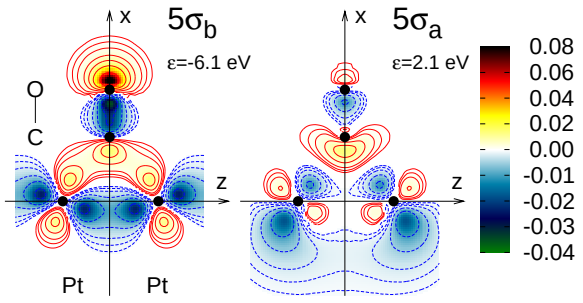

FIG. 4: (Color online) Two dimensional contour plot of the charge density of $5\sigma_b$ (left) and $5\sigma_a$ (right) *KS*-eigenstates calculated at $k_z = 0$. Dots mark the positions of atoms, while solid red (dashed blue) lines are positive (negative) isolevels with the following values of density: ± 0.0005 ± 0.001, ± 0.002, ± 0.005, ± 0.01, ± 0.02, ± 0.05 electrons/(a.u.)^3.

The broadening of molecular features and the presence of several additional peaks indicate a chemical interaction between the molecule and the wire. Interaction between the σ orbitals and Pt states is visible in the projections on the s and p_x orbitals of C and O from -7.5 eV up to 3 eV. In two energy regions, at about 2.1 eV and between -7.5 eV and -6.0 eV there are several large peaks in the s projection and in both the s and p_x projections, respectively, whereas at other energies the projections are smaller while not completely vanishing. The peak centered at about 2.1 eV in the *PDOS* projected on the C s orbital is due to the 5σ orbital and shows that there is a depopulation of the molecular HOMO level (donation). These states are antibonding Pt-CO states while the corresponding bonding states show up as the double-peak feature below E_F, between about -7.5 eV and -6.0 eV. Thus the 5σ orbital is broadened and generates a set of occupied bonding states $5\sigma_b$ below E_F and a set of empty antibonding states $5\sigma_a$ above E_F. Some of the *KS*-eigenstates associated to these peaks are shown in Fig. 4. In this figure we draw a contour plot of the charge density of a $5\sigma_b$ state at -6.1 eV and of a $5\sigma_a$ state at 2.1 eV in the xz plane (which contains both the molecule and the wire). We note that the interaction brings part of the 5σ orbitals below the 1π level, and that there is an orbital mixing between 4σ and 5σ levels. As a consequence, the projections of $5\sigma_b$ states on the s and p_x orbitals of O are higher than those on the s and p_x orbitals of C. These are the same features which characterize the

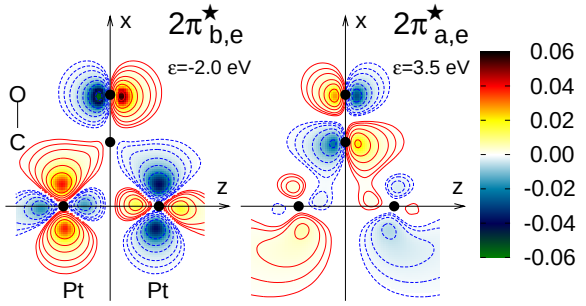

FIG. 5: (Color online) Two dimensional contour plot of the charge density of *KS*-eigenstates (calculated at $k_z = 0$) corresponding to the bonding (left) and antibonding (right) between even $2\pi^\star$ and even Pt states.

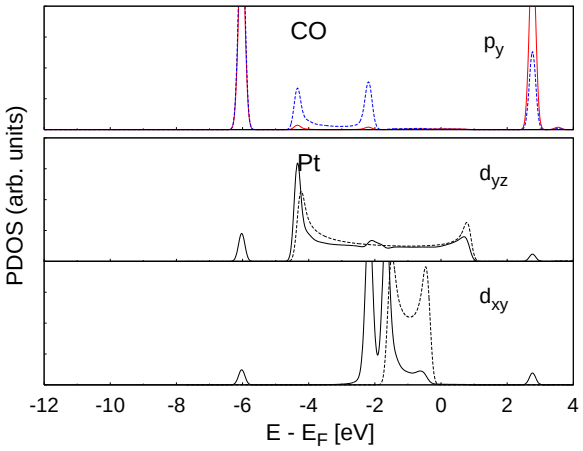

FIG. 6: (Color online) *PDOS* for the *SR-LDA* bridge configuration. The projections are onto the odd atomic orbitals centered on C (solid red lines) and O (dashed blue lines) atoms and on the Pt atoms below the molecule (solid line, lower panel). The *PDOS* for the isolated wire are shown with a dashed line.

absorption of CO on transition metal surfaces, well described in the literature (see Ref. 18). The hybridization of the 5σ orbital is mainly with the $m = 0$ bands of the Pt wire, which have predominant $d_{3z^2-r^2}$ character at low energies and s character at energies higher than 0.4 eV. Moreover a smaller, but relevant, hybridization of 5σ states with d_{xz} ($|m| = 1$) Pt orbitals is present both in $5\sigma_b$ and in $5\sigma_a$ states.

Broad features and additional peaks due to the hybridization are present also in the p_z *PDOS*. Moreover some hybridization of π levels with Pt states occurs also at -6.3 eV, which is the position of the 1π states. The strong peak at about -2 eV and the weaker features above and below -2 eV are due to bonding hybridization between the even $2\pi^\star$ orbital and the Pt states. The presence of these new states, which we may call $2\pi_b^\star$, shows that the $2\pi^\star$ orbital of CO is partially occupied corresponding to back-donation. The $2\pi^\star$ level broadens between 3.2 eV and 3.6 eV and forms the antibonding $2\pi_a^\star$ states. A contour plot of the charge density associated to the $2\pi^\star$-derived states is shown in Fig. 5, a bonding orbital at -2.0 eV on the left and an antibonding orbital at 3.5 eV on the right. The $2\pi_b^\star$ states have a large contribution from oxygen p_z orbitals, with very low projections on the carbon atom (see also Fig. 3). This is caused by a hybridization between the 1π and $2\pi^\star$ orbitals of the molecule due to its interaction with the wire, and has been well characterized for CO adsorbed on metal surfaces.[18] The $2\pi_b^\star$ hybridization at -2 eV involves both $m = 0$ (s and $d_{3z^2-r^2}$) and $|m| = 2$ ($d_{x^2-y^2}$) Pt states, and because of this interaction a relevant portion of the $d_{x^2-y^2}$ *PDOS* moves outside the energy range of the wire $|m| = 2$ band. The $|m| = 1$ (d_{xz}) states instead give a much smaller contribution at -2 eV and interact in a wider energy range between -4 eV and -2 eV.

In Fig. 6 we show the *PDOS* projected on the *odd* atomic orbitals. As found in the even π interaction, in the *PDOS* projected onto the p_y orbitals of C and O two peaks correspond to the odd 1π molecular level at -6 eV and to the odd $2\pi_a^\star$ state at 2.8 eV, while additional peaks are caused by interaction. Here we find two new peaks below E_F, one at -4.3 eV and the other at -2.2 eV. They correspond to the odd $2\pi_b^\star$ levels and their splitting reflects the different hybridization of the $2\pi^\star$ orbital with distinct bands of the wire. The peak at -4.3 eV is present only in the *PDOS* projected on d_{yz}, while the peak at -2.2 eV is essentially due to an hybridization with the $|m| = 2$ band, since the corresponding d_{xy} peak is much stronger than the one in the d_{yz} *PDOS*. As noticed in the even *PDOS*, this strong interaction brings some charge in the $2\pi^\star$ molecular state and perturbs the *PDOS* of the wire, especially the $|m| = 2$ component (d_{xy} in the odd case) where a lot of states are now outside the energy range of the clean wire $|m| = 2$ band.

With addition of *SO* in the *FR* case this donation/back-donation picture does not change. Now states fall into the two irreducible representations Γ^3 and Γ^4 of the double group C_s^D and it is not possible to separate even and odd states. Since in the absence of magnetization time reversal symmetry holds, there is a (Kramers) degeneracy between the Γ^3 band at k_z and the Γ^4 band at $-k_z$. Therefore we can analyze the CO-Pt nanowire system by focusing on bands belonging to one of the two symmetries, for instance the Γ^3 bands.[50] In C or in O there are four *FR* atomic orbitals that transform according to Γ^3, one derived from the s ($l = 0$) state, with $(j, j_y) = (1/2, 1/2)$ and three derived from the p ($l = 1$) states, with $(j, j_y) = (1/2, -1/2)$, $(3/2, -1/2)$, and $(3/2, 3/2)$.

In Fig. 7 we show the *PDOS* projected onto these four Γ^3 atomic orbitals. The molecular levels can be easily identified. At lower energies two sharp peaks are at -22.4 eV (not shown) and at -10.5 eV in all the four *PDOS* and correspond to the 3σ and 4σ *SR* states, re-

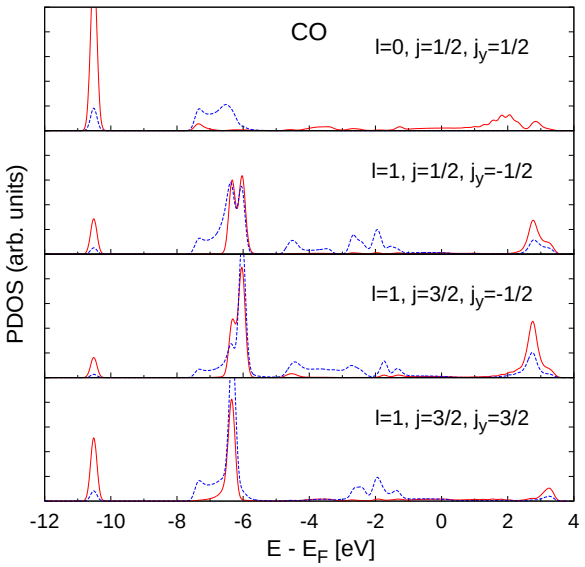

FIG. 7: (color online) *PDOS* for the *FR-LDA* bridge configuration (wire along y, see text). The projections are on the Γ^3 symmetry *FR* atomic orbitals of C (solid red lines) and O (dashed blue lines).

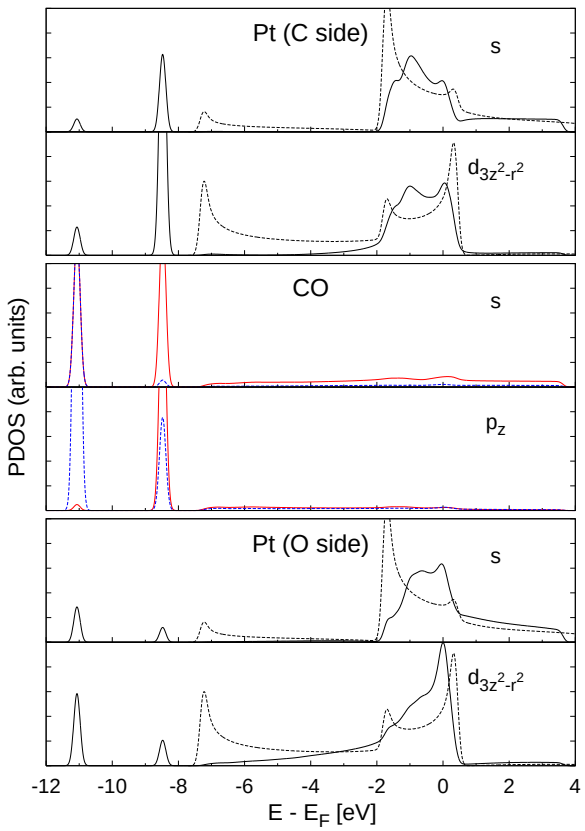

FIG. 8: (Color online) *PDOS* for the *SR-LDA* substitutional configuration. In the central panel the projections are on $m = 0$ atomic orbitals centered on C (solid red lines) and O (dashed blue lines) atoms. In the top (bottom) panel the projections on $m = 0$ atomic orbitals of the Pt atom next to the C atom (O atom) are indicated by solid lines, while the corresponding *PDOS* of the isolated wire are superimposed with dashed lines.

spectively. Two other peaks are close together (-6.3 eV and -6.0 eV) and are both present in the *PDOS* projected onto the two states with $l = 1$ and $j_y = -1/2$, but only the low energy peak is evident in the *PDOS* projected onto the $j_y = 3/2$ state. The position of these two peaks coincides with the even and odd 1π states observed in the *SR PDOS*. The odd 1π state (-6.0 eV) has very low projection onto the $j_y = 3/2$ state since the former is oriented along the xy direction, while the latter is made up of $m = 1$ orbitals, that are oriented in the xz plane (the quantization axis is y). The broad feature between -7.3 eV and -6.2 eV, which is present in all four *PDOS*, can be distinguished from the neighbouring 1π peaks since it has much more weight on the O atom rather than on the C atom, similar to the $5\sigma_b$ *SR* states (see *PDOS* of Fig. 3). Therefore we can identify this feature as the *FR* analog of the $5\sigma_b$ states, which are in the same energy range in the *PDOS* projected on the s and p_x orbitals. Above the Fermi energy, we can identify the empty $5\sigma_a$ antibonding states which give rise to the broad peak at about 2 eV in the $j_y = 1/2$ *PDOS*.

In the energy range between -4.3 eV and -1.1 eV we find some features which are more evident in the $l = 1$ components of the *PDOS*, and have very low weight on the C orbitals. In the *SR* case the energy range of the $2\pi_b^\star$ states goes from -4.4 eV (lowest peak in the p_y *PDOS* of Fig. 6) to about -1 eV (tail of the even $2\pi_b^\star$ peak in the p_z *PDOS* of Fig. 3) and they have very low projections on the carbon, thus we can identify these features in the *FR PDOS* as the *FR* analog of those states. The corresponding even and odd $2\pi^\star$ antibonding states are responsible for the peaks at 3.2 eV and 2.8 eV, respectively. Although their splitting is too small to be resolved in a single *PDOS* with this value of the smearing, only the even peak (such as the even 1π) is evident in the $j_y = 3/2$ *PDOS*, while both are present in the $l = 1$, $j_y = -1/2$ *PDOS* and both have much smaller weight in the $l = 0$ component. We can therefore conclude that although *SO* changes the symmetry of the orbitals, the mechanism of donation and back-donation still describes well the bonding between the molecule and the wire.

B. Substitutional CO

In the substitutional configuration (see Fig. 1) the rotational symmetry is preserved, hence *SR* states with different m cannot hybridize. Therefore we can study the interaction by focusing on the *PDOS* projected on $m = 0$ and $|m| = 1$ orbitals only (Fig. 8 and Fig. 9, respectively), disregarding $|m| = 2$ states that are not present in the molecular levels of CO. The 4σ and 5σ molecular levels give rise to two peaks at -11.0 eV and at -8.5 eV in

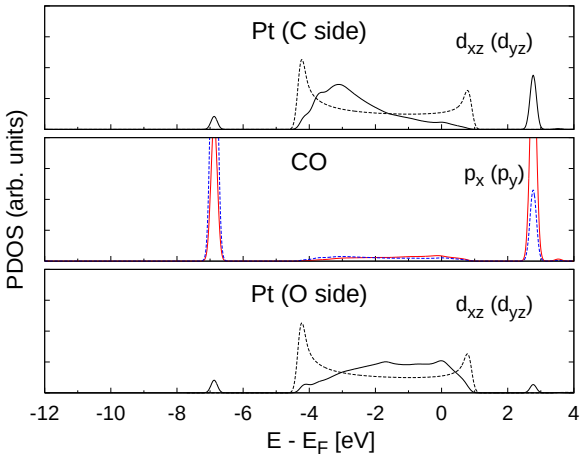

FIG. 9: (Color online) *PDOS* for the same system as in Fig. 8, but here the projections are on $|m| = 1$ atomic orbitals.

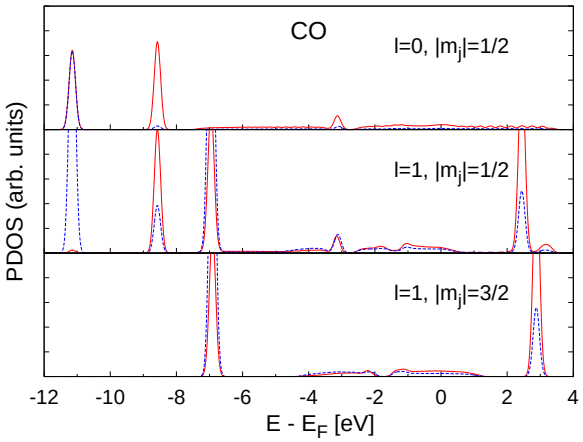

FIG. 10: (Color online) *PDOS* for the *FR-LDA* substitutional configuration. The projections are on the $|m_j| = 1/2$ and $|m_j| = 3/2$ *FR* atomic orbitals of C (solid red lines) and O (dashed blue lines). In the case $l = 1$, $|m_j| = 1/2$ the *PDOS* projected onto states of different j^2 have been added.

the C and O s and p_z *PDOS*. As in the bridge configuration, the $5\sigma_b$ level is lower than the 1π derived level (see below). We do not find here isolated peaks above E_F which correspond to the antibonding $5\sigma_a$ states, but an almost flat plateau which extends in the whole energy range of the $m = 0$ bands of Pt. The hybridization between the 5σ CO orbital and the Pt states is different on the two sides of the molecule, as can be seen comparing the *PDOS* projected onto the $m = 0$ orbitals centered on the two opposite Pt atoms. At -8.5 eV the 5σ CO orbital is more coupled to the Pt on the C side (especially via $d_{3z^2-r^2}$ states), and this causes a higher depopulation of $m = 0$ states between -7.3 eV and -2 eV on the Pt next to the C atom with respect to the Pt on the O side.

The *PDOS* projected onto the $|m| = 1$ (p_x or p_y) orbitals of C and O are reported in Fig. 9 and show two peaks due to the π molecular states, one at -6.8 eV (1π) and another at 2.8 eV ($2\pi^\star$). However, in contrast with the bridge case, instead of new intense peaks below the Fermi energy, we find in the substitutional case a plateau which spans the whole energy range of the Pt wire $|m| = 1$ band.

Although the hybridization with Pt states is different from the bridge geometry, donation/back-donation is present here too. In fact a portion of the plateau in the *PDOS* on $m = 0$ states extends above E_F, while the plateau on the $|m| = 1$ *PDOS* lies mainly below E_F. In order to have an estimate of the donation we can consider the integral (from $-\infty$ to E_F) of the *PDOS* on the C and O orbitals forming σ states in the molecule (s plus p_x in the bridge geometry, s plus p_z in the substitutional). This integral gives 5.3 both in the substitutional and bridge geometries, while in the isolated molecule it gives about 5.9. Estimating in the same way the amount of back-donation, by integrating the *PDOS* on the orbitals which form the π states (p_z plus p_y in the bridge geometry, p_x plus p_y in the substitutional), we find 4.7 electrons both in the substitutional and in the bridge geometry, to be compared to the value of 3.9 obtained with the isolated CO.

In the *FR* case we can label states according to the total angular momentum m_j, and hybridization occurs only among states with the same m_j. In Fig. 10 we report the *PDOS* projected onto the *FR* atomic orbitals of C and O separated according to the values of l and m_j of the spin-angle function. The peaks in these figures can be easily identified and their position compared with that of the *SR* case. In addition to the molecular σ levels present only in the *PDOS* on the $|m_j| = 1/2$ states at -23.7 eV (not shown), -11.2 eV and -8.6 eV, there are two peaks in the $l = 1$, $|m_j| = 1/2$ *PDOS*, one at -7 eV and another at 2.4 eV. They can be matched with the two peaks at -6.9 eV and at 2.8 eV in the $l = 1$, $|m_j| = 3/2$ *PDOS*, and correspond to the *SO* split 1π and $2\pi^*$ states of the molecule. With respect to the isolated molecule, the 1/2-3/2 splitting of the π states is enhanced by the interaction with the Pt states, especially for the $2\pi^\star$ states.

As in the *SR* case, the interaction between the molecule and the wire is visible here as a plateau which extends in a wide energy range. In the *PDOS* projected onto the $l = 0$, $|m_j| = 1/2$ states the plateau extends between -7 eV and 3 eV, and is due to the hybridization between the 5σ orbital with the $|m_j| = 1/2$ bands of the Pt nanowire. The small peak at about -3.3 eV and the gap just above it are due to an anticrossing of the $|m_j| = 1/2$ bands (see Ref. 21), which generates new peaks and gaps in the *FR-DOS* of the Pt nanowire. In the *PDOS* projected on the $l = 1$, $|m_j| = 3/2$ states there is a plateau between -4.2 eV and 0.8 eV due to the hybridization between π-derived states and $|m_j| = 3/2$ states of Pt. This plateau is localized in the same energy range as

that of the *SR* π-$|m| = 1$ bands, slightly increased by the spin-orbit splitting of the $|m| = 1$ band. A hybridization gap of the $|m_j| = 3/2$ band of Pt is visible just above -2 eV. In the *PDOS* projected on $l = 1$, $|m_j| = 1/2$ states we find contributions from both σ-derived an π-derived states. In summary, also in the substitutional geometry we can conclude that the donation/back-donation model gives a good description of both the *SR* and *FR* electronic structure. Near the Fermi level the changes caused by *SO* are not large in extent, but still quite visible in the electronic structure. This will reflect on the ballistic transport properties, which are discussed in the next Section.

V. BALLISTIC CONDUCTANCE

In this section we present the transmission of an infinite ideal platinum chain as a function of energy, for the two CO adsorption geometries discussed above, purposely without tips but with the adsorbed molecule as the sole scatterer. This idealized transmission measures the amount of obstacle posed by the molecule to electron free propagation, in addition to that, molecule-independent, caused by the tip-wire contacts – which as was said are left out here.

The transmission is calculated with the method developed in Refs. 21,35,40, where the self-consistent potentials for the left lead, for the scattering region and for the right lead are calculated using the geometries shown in Fig. 1. The self-consistent potential of one unit cell of the Pt chain in the leftmost part of the supercell is used to calculate the generalized Bloch states of the left and right leads, while the rest of the supercell is the scattering region. We checked that the generalized Bloch bands with real wavevector of the Pt chain calculated with this potential perturbed by CO match those calculated with the exact potential within 0.05 eV.

The *SR* transmission T_{SR} as a function of energy for the bridge geometry is shown in the upper panel of Fig. 11. In the same plot we display also the *FR* transmission T_{FR} for selected energies and the number of channels available for transport (N_{SR} in the *SR* case and N_{FR} in the *FR* case). At the Fermi level four (spin-degenerate) *SR* channels are available, three even and one odd. The $|m| = 2$ bands do not cross $E_{\rm F}$, hence they do not contribute to the conductance. The odd $|m| = 1$ band is almost perfectly transmitted, while the even $|m| = 1$ band and the two $m = 0$ bands are partially reflected. The resulting conductance is $G_{SR} = 6.6\ e^2/h$, to be compared with the value $8\ e^2/h$ of the clean wire. The *FR* conductance, $G_{FR} = 6.5\ e^2/h$, is quite close to the *SR* value because, although the *SO* splitting of the $|m| = 2$ bands brings one two-fold degenerate channel (with $|m_j| = 5/2$) close to $E_{\rm F}$, this additional channel is poorly transmitted (see later) and does not modify the conductance. These values of conductance are close to those found in the on-top geometry: $G = 6.1\ e^2/h$ in both *SR* and *FR* calculations.

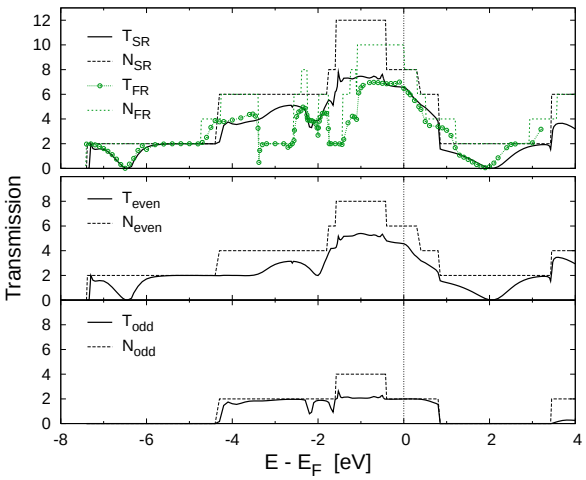

FIG. 11: (Color online) Electron transmission for the bridge geometry. In the top panel the *SR* (*FR*) transmission T_{SR} (T_{FR}) is displayed with solid lines (green circles), while the number of channels N_{SR} (N_{FR}), which equals the transmission of an ideal monatomic chain, is shown with dashed lines (short dashed green lines). In the bottom panel we separate the even and odd components of the *SR* transmission, $T_{\rm even}$ and $T_{\rm odd}$ (above and below, respectively), as well as the number of even and odd channels, $N_{\rm even}$ and $N_{\rm odd}$.

The energy dependent transmission shows instead more pronounced differences between *SR* and *FR* results. In the *SR* case we can separate the contribution of the even and of the odd states (central panel and bottom panel of Fig. 11, respectively), while in the *FR* case states belonging to the Γ_3 or to the Γ_4 representations have the same transmission. We discuss first the *even* contribution to the transmission, trying to establish a connection with the features in the *PDOS* projected on the corresponding atomic orbitals in Fig. 3 of Sec. IV A. Below -4.3 eV there is only one $m = 0$ channel which is almost perfectly transmitted above -5.5 eV, while it is partially reflected at lower energies and totally reflected at -6.4 eV. This happens both in the *SR* and in the *FR* cases. We note that this energy corresponds to the position of the even 1π states, which are rather localized on the CO and on the two neighboring Pt atoms and are responsible for the large mismatch between the $m = 0$ *PDOS* of those two Pt atoms and the corresponding *PDOS* of a Pt atom distant from CO (compare solid and dashed lines in the s and $d_{3z^2-r^2}$ *PDOS* of Fig. 3) At higher energies, where in principle a new even channel (with $|m| = 1$) becomes available, the even contribution to the transmission grows significantly only after -3.3 eV, while below this energy only the $m = 0$ channel is transmitted. Actually, in the energy region between -4.2 eV and -2.1 eV, the even $|m| = 1$ states of the wire are involved in the hybridization with the $2\pi^\star$ molecular orbital and therefore they do not transmit (compare the *PDOS* projected on the d_{xz} orbital with that projected on $d_{3z^2-r^2}$, in Fig. 3: in

this energy range, the matching with the *PDOS* of the Pt distant from CO is better in the case of $d_{3z^2-r^2}$ orbitals rather than d_{xz} orbitals).

Above -2 eV the $2\pi_b^\star$ hybridization has more weight on the $m = 0$ states of Pt than on $|m| = 1$ states, hence the rise of transmission between -2 eV and -1.8 eV has to be ascribed to a better transmission of the $|m| = 1$ channel, rather than to the additional $m = 0$ channel that is present from -1.8 eV onwards. Actually both $m = 0$ channels transmit only partially in this region, and together contribute just for about one half the value of $T_{\rm even}$. Between -1.6 eV and -0.4 eV also the even $|m| = 2$ channel becomes available, but the transmission grows only slightly and remains much smaller then the number of available channels. The bad transmission of $|m| = 2$ states can be easily related to the large mismatch between the $d_{x^2-y^2}$ *PDOS* of the two Pt atoms next to the molecule and that of a Pt atom distant from CO. Between -1.7 eV and -1.5 eV there is also a large difference between *SR* and *FR* transmission since the anticrossing of the 1/2 and 3/2 bands removes several channels from that energy region decreasing the *FR* transmission. Above -0.4 eV the $|m| = 2$ channel is not available anymore and we find a small drop in transmission, which then remains almost constant up to $E_{\rm F}$. From $E_{\rm F}$ up to 0.8 eV the transmission decreases regularly, since first the $|m| = 1$ channel (at 0.4 eV) and then one of the two $m = 0$ channels (at 0.8 eV) disappear. Above 0.8 eV only the $m = 0$ channel with predominant s character is present: its transmission vanishes completely at 2.1 eV and it shows a dip about that energy. This energy value coincides with the position of the $5\sigma_a$ states (see the *PDOS* projected onto the s orbitals in Fig. 3). This dip is present also in the *FR* transmission although it is slightly shifted towards lower energies.

The odd channels are available and can contribute to the transmission between -4.3 eV and 0.8 eV. The $|m| = 1$ channel has good transmission in the whole energy range except for two narrow dips near -2 eV. The lowest dip corresponds to the odd $2\pi_b^\star$ peak present at that energy, while the position of the highest can be matched with the energy of a strong peak in the *PDOS* projected on the d_{xy} states of Pt (which does not correspond to any peak in the *PDOS* of C or O). As for the even $|m| = 2$ channel, also the odd $|m| = 2$ channel is almost blocked because the corresponding Pt states are more perturbed by the interaction with the $2\pi^\star$ orbitals of CO. This difference in the transmission properties between $|m| = 1$ and $|m| = 2$ odd channels could be predicted by the *PDOS* reported in Fig. 6: in fact, the d_{yz} *PDOS* looks similar to that of a Pt atom of the pristine nanowire, while the d_{xy} *PDOS* does not match at all the original *PDOS* of the wire.

A feature similar to the dip at 2.1 eV has already been observed in the transmission curve calculated for gold nanowires with CO absorbed on-top,[41,42] but in that case the dip is closer to the Fermi energy. This causes a drop in the predicted conductance of the Au nanowire when

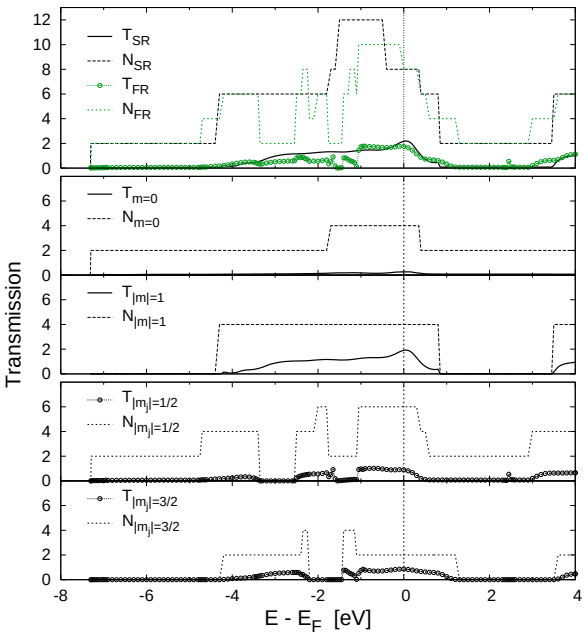

FIG. 12: (Color online) Electron transmission for the substitutional geometry. In the top panel the *SR* (*FR*) transmission T_{SR} (T_{FR}) is displayed with solid lines (green circles), while the number of channels N_{SR} (N_{FR}), is shown with dashed lines (short dashed green lines). In the middle (bottom) panel we separate the *SR* (*FR*) transmission and number of channels according to the angular momentum $|m|$ ($|m_j|$). The contribution from $|m| = 2$ ($|m_j| = 5/2$) channels to the total *SR* (*FR*) trasmission is practically zero, hence it is not shown (see text).

CO is adsorbed because, in that case, the $6s$ state is the only conducting channel left at $E_{\rm F}$. Instead, in the pristine Pt nanowire three more channels are available for conduction, and the dip in the $m = 0$ transmission caused by CO adsorption lies above the Fermi level.

The *SR* and *FR* total transmissions as a function of energy for the substitutional geometry are shown in the top panel of Fig. 12. In this geometry we find a conductance of about 2.2 e^2/h, much smaller than in the bridge geometry. Actually at the Fermi level the transmission of the two degenerate $|m| = 1$ channels is about one half and that of the $m = 0$ channels is quite small (slightly above 0.1). In the other energy regions the transmission is even lower, since the $m = 0$ channels are almost totally blocked and the transmission of the $|m| = 1$ channels remains always below one half. The 5σ-derived states could in principle transmit because they hybridize with Pt states, but actually this is not the case since the coupling of the left Pt to CO is quite different from that of right Pt, as noted before in Sec. IV B. Moreover, the transmission due to the $|m| = 2$ bands of Pt (not shown here) is close to zero, since the CO has no states with matching symmetry.

Thus the *SR* and *FR* calculations give similar results

also for the substitutional geometry; the calculated *FR* value of the conductance is 1.7 e^2/h to be compared with $G = 6.5\ e^2/h$ for the upright bridge. In the substitutional case the contributions from the $|m_j| = 1/2$ and the $|m_j| = 3/2$ channels are almost equal, in agreement with the fact that in the *SR* case only the $|m| = 1$ channels contribute to transmission.

We can pinpoint some dips specific to the *FR* energy dependent transmission, that are due to the *SO* induced splittings of the bands. They are evident if we look separately at the $|m_j| = 1/2$ and $|m_j| = 3/2$ contributions to the total number of available channels: the former goes to zero between -3.4 eV and -2.5 eV, while the latter vanishes between -2.2 eV and -1.4 eV. The $|m_j| = 5/2$ contribution to the transmission (not shown) is almost zero, since the $|m_j| = 5/2$ channels have $|m| = 2$ orbital components that are completely blocked by the CO. It should be pointed out here that the details of all channels will be modified by the onset of magnetism,[23,43] and this could in principle modify the ballistic conductance of our system. This aspect however is beyond the scopes of this work.

Although as was said above our conductance values cannot be directly compared with experimental data because they do not include the effect of the tips, they do indicate that in the substitutional configuration the conductance is about 3 times lower than in the upright bridge configuration,[15] where at difference with the substitutional the $m = 0$ channels are not so strongly reflected. The Pt states with angular momentum $|m| = 2$ are (more or less strongly) blocked in both cases, but for different reasons: in the bridge geometry they interact more with CO and this perturbs a lot the $|m| = 2$ *PDOS* on the neighbouring Pt; in the substitutional there is no CO orbital with the matching symmetry and thus the $|m| = 2$ channel is totally blocked by the molecule. Anyway, since these states fall below the Fermi level, their interaction with the molecule does not influence the conductance. The *FR* conductance does not differ substantially from the *SR* value because the $|m_j| = 5/2$ channels (which could in principle give rise to an increased conductance, since the corresponding *FR* band approaches the Fermi level) are almost completely blocked both in the upright bridge and in the substitutional case, and because there are no *SO*-induced gaps near the Fermi level.

VI. CONCLUSIONS

We have explored the bonding mechanism of a CO molecule onto a Pt monatomic nanowire. We found that in the bridge (and also in the on-top[25,26]) configuration the Blyholder model is appropriate to describe the electronic structure and the molecule-wire bonding. The HOMO and LUMO molecular orbitals are mainly involved in the bonding and strongly hybridize with Pt states forming bonding/antibonding states. As a consequence, from the 5σ molecular orbital some charge transfers to the wire, which in turn back-donates some of the charge, partially filling the $2\pi^\star$ orbitals of the molecule. The substitutional geometry has quite a high energy hence it could be a realistic configuration only when the wire is under high strain and almost broken. Also in this case there occurs a hybridization between the Pt states and the CO molecular orbitals which gives rise to a donation/back-donation process. We showed that the inclusion of *SO* coupling, which strongly modifies the electronic band structure of the Pt wire, does not change very much the interaction mechanism and strength between the CO molecule and the wire.

The adsorption of CO on bridge (and also on-top) geometry should not affect much the chain ballistic conductance, since the Pt states mainly involved in the interaction with CO — and therefore partially or totally reflected — are located mainly below or above the Fermi level. In the substitutional geometry instead the molecule can partially transmit only $|m| = 1$ states, while all other channels are blocked.

Our findings confirm the speculation by Kiguchi et al.[9] based on the measured conductances of transition metal nanocontacts, namely that the Blyholder model rules the adsorption strength of CO. Regarding the transport properties, our results agree with those of Strange et al.[15] in predicting that a considerable reduction of the ballistic conductance can be obtained when CO goes substitutional, and that the main conducting channel comes from a Pt $|m| = 1$–$2\pi^\star$ hybridization (while $m = 0$ states should not be conducting). Unlike previous calculations, we carefully examined *SO* effects on the intrinsic (tipless) conductance and find that, for the specific case of the non-magnetic Pt nanocontact with an adsorbed CO molecule, a treatment of the electronic structure at the *SR* level was basically adequate to catch the effects on the conductance when bonding CO to the nanowire.

Acknowledgments

This work has been supported by PRIN Cofin 2006022847, as well as by INFM/CNR "Iniziativa trasversale calcolo parallelo". All calculations have been performed on the SISSA-Linux cluster and at CINECA in Bologna, by using the `PWscf` and `PWCOND` codes, contained in the QUANTUM-ESPRESSO package.[28]

[1] N. Agraït, A. L. Yeyati, and J. M. van Ruitenbeek, Phys. Rep. **377**, 81 (2003).

[2] Y. V. Sharvin, Sov. Phys.-JETP **21**, 655 (1965), [Zh. Eksp. Teor. Fiz. 48, 984-985 (1965)].

[3] H. Ohnishi, Y. Kondo, and K. Takayanagi, Nature (London) **395**, 780 (1998).
[4] V. Rodrigues and D. Ugarte, Phys. Rev. B **63**, 073405 (2001).
[5] V. Rodrigues, J. Bettini, P. C. Silva, and D. Ugarte, Phys. Rev. Lett. **91**, 096801 (2003).
[6] A. I. Yanson, G. R. Bollinger, H. E. van den Brom, N. Agraït, and J. M. van Ruitenbeek, Nature (London) **395**, 783 (1998).
[7] R. H. M. Smit, C. Untiedt, A. I. Yanson, and J. M. van Ruitenbeek, Phys. Rev. Lett. **87**, 266102 (2001).
[8] C. Untiedt, D. M. T. Dekker, D. Djukic, and J. M. van Ruitenbeek, Phys. Rev. B **69**, 081401(R) (2004).
[9] M. Kiguchi, D. Djukic, and J. M. van Ruitenbeek, Nanotechnology **18**, 035205 (5pp) (2007).
[10] R. H. M. Smit, Y. Noat, C. Untiedt, N. D. Lang, M. C. van Hemert, and J. M. van Ruitenbeek, Nature (London) **419**, 906 (2002).
[11] S. K. Nielsen, Y. Noat, M. Brandbyge, R. H. M. Smit, K. Hansen, L. Y. Chen, A. I. Yanson, F. Besenbacher, and J. M. van Ruitenbeek, Phys. Rev. B **67**, 245411 (2003).
[12] D. Djukic, K. S. Thygesen, C. Untiedt, R. H. M. Smit, K. W. Jacobsen, and J. M. van Ruitenbeek, Phys. Rev. B **71**, 161402(R) (2005).
[13] M. Kiguchi, R. Stadler, I. S. Kristensen, D. Djukic, and J. M. van Ruitenbeek, Phys. Rev. Lett. **98**, 146802 (2007).
[14] R. Landauer, IBM J. Res. Dev. **1**, 233 (1957).
[15] M. Strange, K. S. Thygesen, and K. W. Jacobsen, Phys. Rev. B **73**, 125424 (2006).
[16] G. Blyholder, J. Phys. Chem. **68**, 2772 (1964).
[17] B. Hammer, Y. Morikawa, and J. K. Nørskov, Phys. Rev. Lett. **76**, 2141 (1996).
[18] A. Föhlisch, M. Nyberg, P. Bennich, L. Triguero, J. Hasselström, O. Karis, L. G. M. Pettersson, and A. Nilsson, J. Chem. Phys. **112**, 1946 (2000).
[19] F. A. Cotton, G. Wilkinson, C. A. Murillo, and M. Bochmann, *Advanced inorganic chemistry 6th ed.* (John Wiley & Sons, New York, 1999).
[20] A. Delin and E. Tosatti, Phys. Rev. B **68**, 144434 (2003).
[21] A. Dal Corso, A. Smogunov, and E. Tosatti, Phys. Rev. B **74**, 045429 (2006).
[22] A. Dal Corso and A. Mosca Conte, Phys. Rev. B **71**, 115106 (2005).
[23] A. Smogunov, A. Dal Corso, A. Delin, R. Weht, and E. Tosatti, Nat Nano **3**, 22 (2008).
[24] S. R. Bahn, N. Lopez, J. K. Nørskov, and K. W. Jacobsen, Phys. Rev. B **66**, 081405(R) (2002).
[25] G. Sclauzero (2006), M. S. thesis, Università degli Studi di Udine.
[26] G. Sclauzero, A. Dal Corso, A. Smogunov, and E. Tosatti, in *FRONTIERS OF FUNDAMENTAL AND COMPUTATIONAL PHYSICS: 9th International Symposium* (AIP, 2008), vol. 1018, pp. 201–204.
[27] P. Hohenberg and W. Kohn, Phys. Rev. **136**, B864 (1964).
[28] S. Baroni, A. Dal Corso, S. de Gironcoli, and P. Giannozzi, websites: `http://www.pwscf.org`, `http://www.quantum-espresso.org`.
[29] W. Kohn and L. J. Sham, Phys. Rev. **140**, A1133 (1965).
[30] J. P. Perdew and A. Zunger, Phys. Rev. B **23**, 5048 (1981).
[31] J. P. Perdew, K. Burke, and M. Ernzerhof, Phys. Rev. Lett. **77**, 3865 (1996).
[32] D. Vanderbilt, Phys. Rev. B **41**, 7892(R) (1990).
[33] A. Dal Corso, Phys. Rev. B **76**, 054308 (2007).
[34] M. Methfessel and A. T. Paxton, Phys. Rev. B **40**, 3616 (1989).
[35] H. J. Choi and J. Ihm, Phys. Rev. B **59**, 2267 (1999).
[36] A. Smogunov, A. Dal Corso, and E. Tosatti, Surf. Sci. **566-568**, 390 (2004).
[37] P. Feibelman, B. Hammer, J. Norskov, F. Wagner, M. Scheffler, R. Stumpf, R. Watwe, and J. Dumesic, J. Phys. Chem. B **105**, 4018 (2001).
[38] N. Oncel, W. J. van Beek, J. Huijben, B. Poelsema, and H. J. Zandvliet, Surf. Sci. **600**, 4690 (2006).
[39] H. Orita, N. Itoh, and Y. Inada, Chemical Physics Letters **384**, 271 (2004).
[40] A. Smogunov, A. Dal Corso, and E. Tosatti, Phys. Rev. B **70**, 045417 (2004).
[41] M. Strange, I. S. Kristensen, K. S. Thygesen, and K. W. Jacobsen, The Journal of Chemical Physics **128**, 114714 (2008).
[42] A. Calzolari, C. Cavazzoni, and M. Buongiorno Nardelli, Phys. Rev. Lett. **93**, 096404 (2004).
[43] A. Smogunov, A. Dal Corso, and E. Tosatti, Phys. Rev. B **78**, 014423 (2008).
[44] S. G. Louie, S. Froyen, and M. L. Cohen, Phys. Rev. B **26**, 1738 (1982).
[45] We used as reference *SR* (*FR*) all-electron configurations $2s^2 2p^2$ ($2s^2_{1/2} 2p^2_{1/2}$) and $2s^2 2p^4$ ($2s^2_{1/2} 2p^2_{1/2} 2p^2_{3/2}$) for C and O, respectively. The core radii for all channels are (1.3, 1.6) and (1.4, 1.6) in the C and O *PP*, respectively. The 3*d* channel potential was treated as local with a core radius of (1.3) (C) and (1.4) (O), respectively. When two core radii are specified, that potential was pseudized in the *US* scheme, with the first radius representing the norm-conserving core radius and the second the *US* one.
[46] The all-electron configurations are the same used in the *SR-LDA* case. The core radii of Pt are (1.8, 2.2) for the 5*d* orbitals, (2.6) for the 6*p* and (2.4) for the 6*s*. For the 2*s* orbitals of C the core radius is (1.4, 1.6), while for all the other channels we used the same core radii of the *LDA PP*. The non-linear core correction[44] has been included in all the *PP*.
[47] We performed a test calculation with 25 Pt atoms for both bridge and substitutional *SR* geometries (see Sec. III) and obtained very good agreement with the 17 Pt calculations. Around the Fermi energy the difference in the calculated transmission remains below 1%, while in the overall energy range the difference is at most 3%.
[48] In the structural optimizations we require that each component of the force on the C and O atoms gets lower than 1 mRy/a.u. . In the bridge and on-top geometries the C and O atoms are constrained to move on the axis perpendicular to the wire (x axis), while in the substitutional case we keep them aligned with the wire (hence on the z axis). In the tilted bridge configuration, the C and O atoms can move on the xz plane.
[49] In the SUBS-oxygen case we start with the O atom next to a Pt atom and the C atom distant from the Pt atom at the other side. For $d_{\mathrm{Pt-Pt}} < 9.0$ Å the final configuration is the same as in the SUBS-carbon case (where we start with O distant from Pt), since the energy of that configuration is significantly lower.
[50] The atomic orbitals suited for the projection of states with Γ^3 symmetry can be chosen among spinors which are eigenstates of the total angular momentum J^2, (with eigenvalue $j(j+1)$) and of its projection along y, J_y (with eigenvalue j_y). These states, labeled with (j, j_y), transform according to the Γ^3 or Γ^4 irreducible representations.